ELSEVIER

Journal of Wind Engineering
and Industrial Aerodynamics 84 (2000) 47–64

JOURNAL OF wind engineering AND industrial aerodynamics

www.elsevier.com/locate/jweia

Large eddy simulation of turbulent flows in periodically grooved channel

Kyung-Soo Yang*

Department of Mechanical Engineering, Inha University Inchon, 402-751, South Korea

Received 6 September 1998; received in revised form 28 April 1999; accepted 11 May 1999

Abstract

In this study, turbulent flows in periodically grooved channel are investigated by large eddy simulation (LES). Especially, a parametric study is carried out to investigate effects of length and depth of a groove on large-scale flow structures. Comparison of LES results with those of DNS for one test case reveals a good agreement even though the number of grid points of the LES is only 6.5% of that of DNS. This confirms that LES is a suitable tool for a parametric study of turbulent flows. The subsequent parametric study using LES shows that the large-scale turbulent structures are significantly affected by the geometry of the groove. Especially, when the length of the groove is short such that the recirculation region occupies the entire groove, the turbulent flow in the groove becomes very weak in both mean and fluctuation quantities.

Keywords: Large eddy simulation; Turbulent flow; Groove; Parametric study

1. Introduction

Turbulent flow in periodically grooved channel (PGC) is often found in various applications. Examples are air flow as a coolant between two parallel printed circuit boards (PCB) on which aligned chips are mounted, wind around a row of buildings, and flow over surface roughness related to erosion on pipelines, to name a few. Here, we consider a channel with rectangular grooves installed periodically in the direction of the main flow (Fig. 1). The grooved-channel flow contains all the flow structures related to complex geometry such as wall-shear layers, free-shear layers, and recirculation regions. Furthermore, from the numerical point of view, PGC allows one to easily

* Tel.: 82-32-860-7322; fax: 82-32-868-1716.
E-mail address: ksyang@dragon.inha.ac.kr (K.-S. Yang)

0167-6105/00/$ - see front matter
PII: S0167-6105(99)00049-5

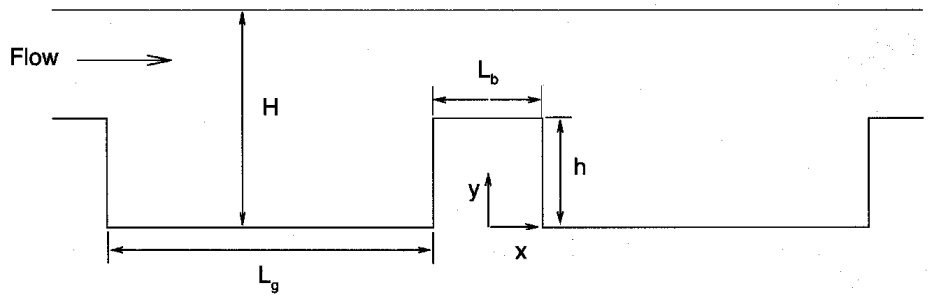

(a)

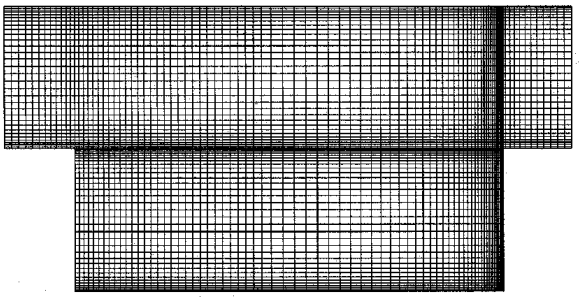

(b)

Fig. 1. (a) Physical configuration (a side view); (b) a typical computational grid at a x–y plane.

obtain statistically steady flow, and the controversial inflow/outflow boundary conditions can be replaced with the periodic one. Therefore, turbulent flow in PGC can be considered as a basic model for the flows mentioned above.

The main difference between the grooved-channel flow and the flow over a backward-facing step or over a single obstacle is that there is no redeveloping region in the former. Thus, large-scale structures are significantly affected by the shape and size of the groove, and it is not possible to understand the mechanisms of heat and mass transfers in the grooved-channel flow without prior knowledge of fluid mechanics involved. Experimental investigations on the flows similar to the grooved-channel flow have been carried out [1,2]. However, experimental data on a recirculating turbulent flow contained in a small groove are very rare. Okamoto and Nakaso [3] performed an experimental investigation on the flow over square ribs mounted on a flat plate in the direction of the main flow. Their objective was to obtain the optimal rib span in order to maintain the freestream turbulence. Yamashita et al. [4] experimentally studied boundary-layer flows over a flat plate with a single groove. However, these flows are rather specific and cannot be regarded as the "basic" grooved-channel flow. Larminar-turbulent transition in PGC has been numerically studied [5–7]. However, to the author's knowledge, none has been done on turbulent flows in PGC. In the field of wind engineering, both experimental and numerical investigations were performed on the flows around cubic obstacles in turbulent boundary layers. See Refs. [8,9].

In this investigation, large-eddy simulation (LES) is employed to study turbulent flows in PGC. Especially, a parametric study is carried out to study effects of length and depth of a groove on large-scale flow structures, which also have their relevance to wind engineering problems. Although direct numerical simulation (DNS) can provide the most accurate flow data, it is not suitable for a parametric study where different values of geometrical dimensions and flow parameters must be considered, due to the limited computing resources currently available. However, DNS data can serve as benchmark data to verify accuracy and effectiveness of LES. In this study, DNS was performed for one case and both qualitative and quantitative evaluations were made for the corresponding LES. After such verification, LES was utilized to obtain detailed flow data for various different cases.

2. Methodological and numerical considerations

The objectives of this study are to identify the effects of length and depth of a groove on large-scale flow structures, and to generate detailed flow data for each case. Here, the Reynolds number (Re) is based on the mean bulk velocity (U_m) between the upper and the lower walls of the channel and the distance between the two walls ($H - h$). Its value is approximately fixed as 6900. This means that the volume flux is approximately equal for each case. Table 1 summarizes all the cases computed in this study. Special attentions are paid to Cases 3,4,5 and 7 where the length of the groove (L_g) varies, and to Cases 4 and 6 where the depth of the groove varies. These two quantities characterize the geometry of PGC. Depending upon their relative values, it can be regarded as a model flow corresponding to a specific application among those mentioned in the previous section.

2.1. Formulation

All variables are nondimensionalized by U_m and $H - h$. The code uses a nonuniform Cartesian staggered grid in a finite-volume approach. After filtering the

Table 1
Simulation cases. See Fig. 1 for the geometrical symbols, h, H, and L_g. TI and FTT represent the nondimensional Time Interval for averaging and the corresponding flow-through time, respectively. X_g indicates a reattachment length on the bottom of the groove, and X_b denotes a reattachment length on the top of the protruding surface

Case	Algorithm	h/H	L_g/h	Re	Grid No.	$\Delta p/\Delta p_{\text{Case 3}}$	TI	FTT	X_g/h	X_b/h
1	DNS	0.5	15	6830	$384\times168\times72$	—	130	9	5.00	—
2	CDNS	0.5	15	7340	$204\times72\times36$	—	130	9	5.42	0.92
3	LES	0.5	15	6720	$132\times48\times48$	1.0	38.3	2.4	4.84	0.98
4	LES	0.5	7	6680	$132\times48\times48$	1.54	19.7	2.5	3.39	0.81
5	LES	0.5	3	7460	$96\times64\times48$	1.48	19.8	3.1	—	0.12
6	LES	0.25	7	6950	$96\times72\times48$	0.2	9.4	1.7	4.27	0.83
7	LES	0.5	2	6800	$124\times56\times48$	0.31	28.7	3.6	—	0.05

incompressible continuity and momentum equations using a simple volume-average box filter, we obtain the following governing equations for LES:

$$\frac{\partial \bar{u}_i}{\partial x_i} = 0, \tag{1}$$

$$\frac{\partial \bar{u}_i}{\partial t} + \frac{\partial}{\partial x_j}(\bar{u}_i \bar{u}_j) = -\frac{\partial \bar{p}}{\partial x_i} - \frac{\partial}{\partial x_j}\tau_{ij} + \frac{1}{\mathrm{Re}}\frac{\partial^2 \bar{u}_i}{\partial x_j \partial x_j}, \tag{2}$$

where u_1, u_2, u_3 (or u, v, w) are velocities in x_1 (streamwise), x_2 (normal), x_3 (spanwise) directions (or x, y, z), respectively, and p is pressure. The equations must be closed by modeling τ_{ij} term. The volume-average box filter is defined by

$$\bar{u}_i(\boldsymbol{x}, t) = \frac{1}{\Delta x_1 \Delta x_2 \Delta x_3} \int_{x_1-\Delta x_1/2}^{x_1+\Delta x_1/2} \int_{x_2-\Delta x_2/2}^{x_2+\Delta x_2/2} \int_{x_3-\Delta x_3/2}^{x_3+\Delta x_3/2} u_i(\boldsymbol{x}', t)\, d\boldsymbol{x}', \tag{3}$$

where $\boldsymbol{x} = (x_1, x_2, x_3)$ and $d\boldsymbol{x}' = dx_1' dx_2' dx_3'$. See Ref. [10] for details.

2.2. Numerical method

To advance the solution in time, a fractional step method [11] is employed. The time advancement of the momentum equations is hybrid; the convective terms are explicitly advanced by a third-order Runge–Kutta scheme and the viscous terms implicitly by Crank–Nicolson method. A second-order accurate central differencing is utilized for spatial discretization. The code is fully vectorized; it runs at a typical speed of 1.5GFLOPS on NEC SX-3. See Ref. [10] for detailed description of the numerical method used in the code.

2.3. Choice of subgrid-scale model

A dynamic subgrid-scale model (DSGSM) which is a type of eddy viscosity model was chosen for this investigation. In DSGSM, the model constant is not prefixed, but determined as computation progresses. The superiority of DSGSM over the conventional Smagorinsky model has been proven by some researchers [10,12,13]. For detailed description and implementation of DSGSM, see Ref. [10].

2.4. Choice of parameters and boundary conditions

In all cases, periodic boundary conditions were employed in the periodic (x) direction as well as in the homogeneous (z) direction; at the walls, the no-slip boundary condition was imposed. Calculations were carried out using a computational domain with only one groove in order to avoid an excessive computing time which could cost if multiple grooves were included in the domain. This approach is similar to the concept of minimal channel of Jimenez and Moin [14]. The main emphasis is placed on revealing qualitative changes of large-scale flow structures due to the changes of geometric parameters.

A relatively low value of Reynolds number (Re = 6900) was selected to allow the no-slip boundary condition to be imposed at the all solid walls. For higher Re, a larger number of grid points are required to provide a proper resolution near the walls, which results in an excessive computing time. An alternative would be imposing a wall-layer model at the walls. However, this will introduce another uncertainty in the accuracy of computation.

In all cases except Case 7, the streamwise length of the protruding part (L_b) was fixed as $H/2$. The spanwise size of the computational domain was 2H in all cases. The streamwise length of the groove (L_g) is relatively bigger than L_b (see Table 1). This is corresponding to the situation of air flow between two PCBs or flow over wall roughness. One can expect that its large-scale flow structure would be quite different from that of a case with $L_b > L_g$ (Case 7). In the former, the free-shear layer created near the upper downstream corner of the groove is dominant. In the latter, however, the flow inside the groove is very weak, and the conventional "channel" flow dominates.

Unsteady flow in a channel can be classified into one of the following two cases. In one case, mass flux is fixed in time, but pressure difference between inlet and outlet of the channel (Δp) fluctuates. In the other case, mass flux fluctuates while Δp is fixed in time. For the flow geometry under consideration, as long as a finite-volume method is employed, it is not possible to fix mass flux exactly. Thus, the latter approach is adopted for this study. Even though every effort was made to have Re of each case be as close to 6900 as possible, it was inevitable to allow slight differences in Re (see Table 1). The number of control volumes used in each case is also shown in Table 1. In LES, only 6.5% of DNS resolution was used.

3. Results and discussion

3.1. Comparison with DNS

To estimate the accuracy of LES as a research tool, a comparison with DNS data was made first. Case 1 in Table 1 represents the benchmark data obtained by DNS. Detailed sets of data from the DNS are reported elsewhere [15]. Realizations were sampled for 130 nondimensional time interval (TI, Table 1) corresponding to 9 flow-through time (FTT, Table 1. One FTT means the time it would take for a fluid particle with the inlet mean velocity to travel from inlet to outlet of the computational domain.) to reduce the statistical errors in the averaging process. It took about 800 hours of CPU time on a NEC SX-3 for Case 1. For LES, averaging was performed for a relatively short TI to avoid an excessive CPU time. However, it was confirmed that mean velocities and turbulent fluctuations do not change for a longer TI for each LES case reported in Table 1. Case 2 is a simulation without a turbulence model for the same geometry of Case 1, and referred to as coarse-grid DNS (CDNS) hereinafter. CDNS is useful in evaluating the accuracy of LES (Case 3) against the fine-grid DNS (Case 1). Case 3 is corresponding to LES for the same geometry as Case 1 with the difference in Re being approximately 1.6%.

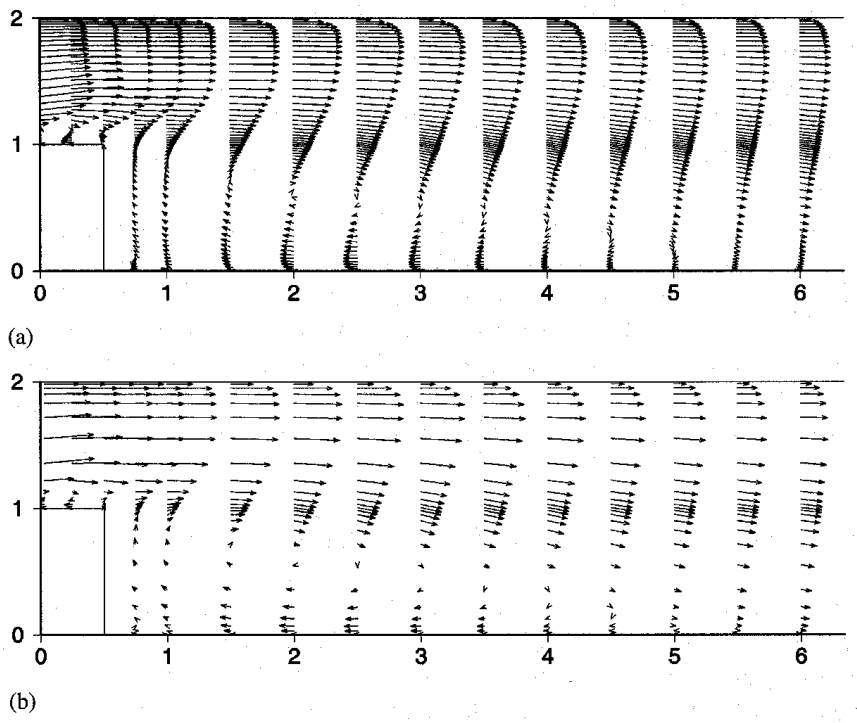

Fig. 2. Velocity vector plots near the upstream corner of the groove: (a) DNS; (b) LES.

Comparison of LES with DNS is made for the quantities averaged both in z and in time. Figs. 2 and 3 show the velocity-vector plots near the upstream and the downstream corners of the groove, respectively. The vectors were scaled independently for each case. One can notice a good agreement in large-scale structures for both cases. Especially, the differences in the reattachment lengths on the bottom of the groove (X_g) and on the top of the protruding surface (X_b) are about 3.2% and 2%, respectively. The secondary eddies in the lower corners of the groove are also well resolved in both cases.

Fig. 4 shows the shear-stress (τ_w) distribution on the lower walls of the channel and the groove. The groove is located between $x = 0.5$ and 15.5. The result of LES is in better qualitative and quantitative agreements with that of DNS than CDNS, even though more finer resolution was in fact applied in CDNS (Table 1). This is an indication of the importance of the subgrid-scale modelling.

In Fig. 5, are shown the averaged streamwise (U) and normal (V) velocities at $x = 2.5$ in the main recirculation region. LES yields better results than CDNS. Especially, LES performs well in the wall- and free-shear layers which are the important regions in turbulence production. LES performs slightly better for V than CDNS. It should be noted, however, that the magnitude of V is much smaller than that of U.

Fig. 6 exhibits the averaged turbulent fluctuations in x ($\overline{u'^2}$) and y ($\overline{v'^2}$), at the same location as in Fig. 5. LES shows definitely better results than CDNS in the most part

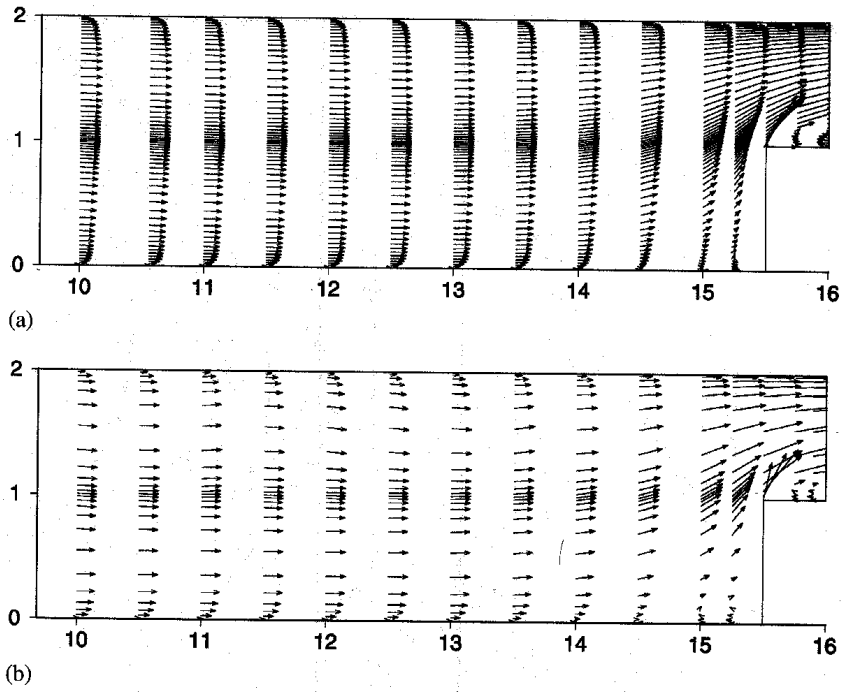

Fig. 3. Velocity vector plots near the downstream corner of the groove: (a) DNS; (b) LES.

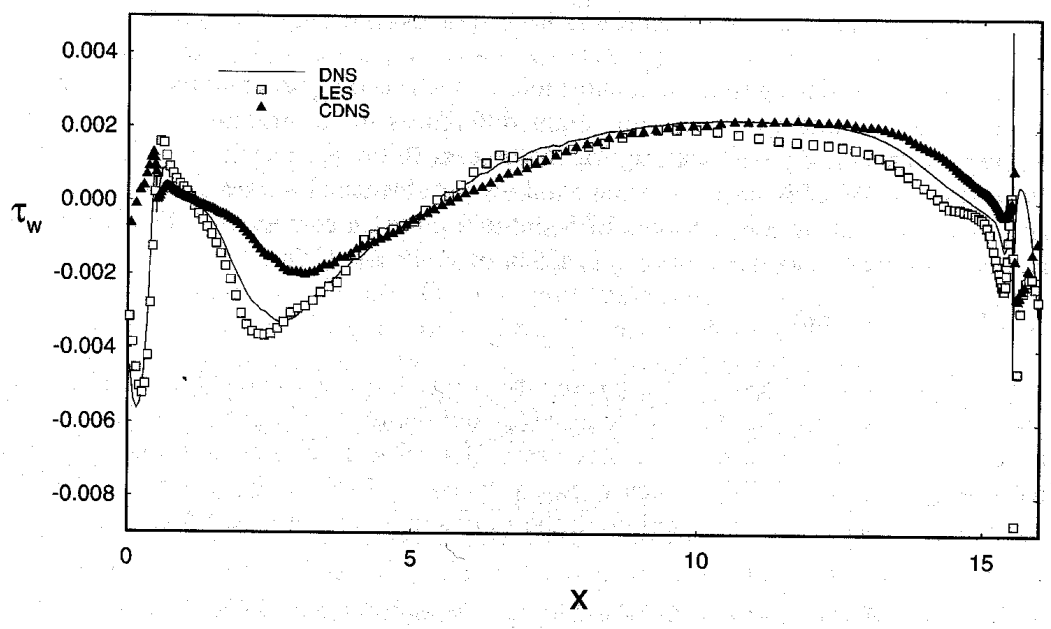

Fig. 4. Comparison of shear stress on the lower walls of the channel and the groove.

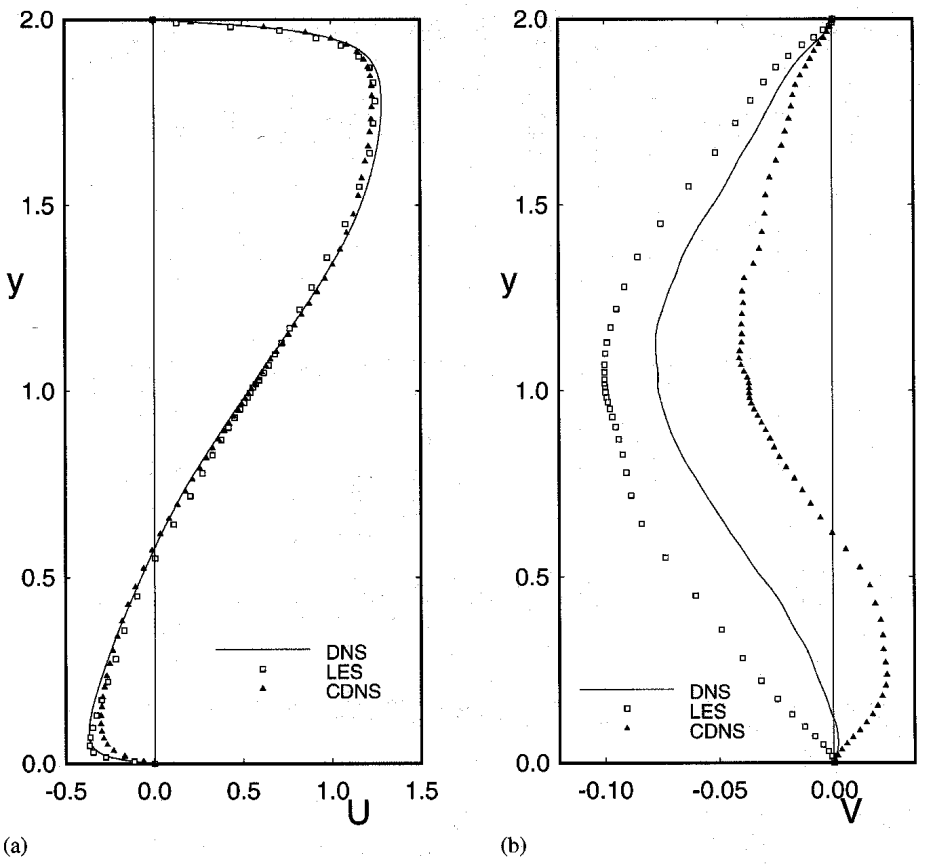

Fig. 5. Profiles of averaged streamwise and normal velocities at $x = 2.5$: (a) U; (b) V.

of the flow. Considering that the magnitudes of such second-order statistics are much smaller than U, and that there are slight differences in Re among the three cases, discrepancies in some parts of the flow field seem to be acceptable.

To summarize, LES has been proven to be a suitable tool for a parametric study on large-scale flow structures because LES shows a good agreement with DNS in mean and second-order statistics using only 6.5% of DNS resolution.

3.2. Parametric study

In this section, the results of a parametric study are presented. Main emphasis is placed on identifying the effects of length (L_g) and depth (h) of a groove on large-scale flow structures. For this purpose, five cases of LES were carried out, and the flow parameters, TI, and FTT of each case are listed in Table 1. In Cases 3–5, and 7, L_g changes while h remains unaltered; the opposite is true in Cases 4 and 6.

3.2.1. Averaged flow fields

Fig. 7(a), (b), (c) and (d) show the averaged velocity fields of Cases 4, 5, 6 and 7, respectively; the vector plots corresponding to Case 3 were already given in

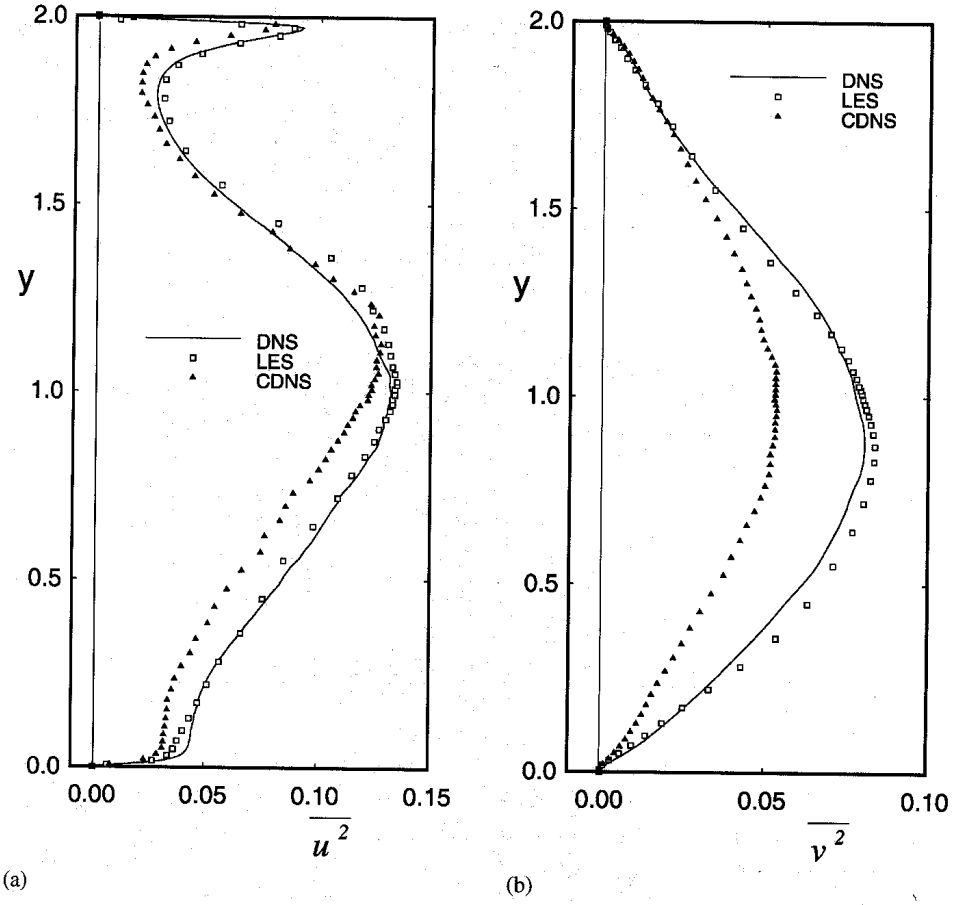

Fig. 6. Profiles of averaged streamwise and normal turbulent fluctuations at $x = 2.5$: (a) $\overline{u'^2}$; (b) $\overline{v'^2}$.

Figs. 2 and 3. In Cases 3, 4, and 6, recirculating regions are present on the top of the protruding surface as well as in the upstream part of the groove. The reattachment lengths of the regions are listed in Table 1. The shorter L_g is, the smaller X_g is. However, in Cases 5 and 7, the main recirculating region occupies the whole groove and reattachment does not occur. Furthermore, there is no recirculating region on the top of the protruding surfaces. In these cases, the magnitude of the averaged velocity is very small in the groove (Fig. 7(b) and (d)). The strength of the recirculating flow is thus weak. Therefore, the whole flow approaches the conventional "channel" flow between two parallel plates $H - h$ apart, to which the "quiet" groove region is attached.

In Case 6, the groove depth is one half of that of Case 4. The size of each recirculating region is accordingly reduced such that the ratio of each dimension to h is not far from that of Case 4 (Table 1). This illustrates the fact that in the range of L_g considered, the overall flow structure does not alter significantly under a moderate change of h. The small difference in X_g and X_b can be explained by the observation

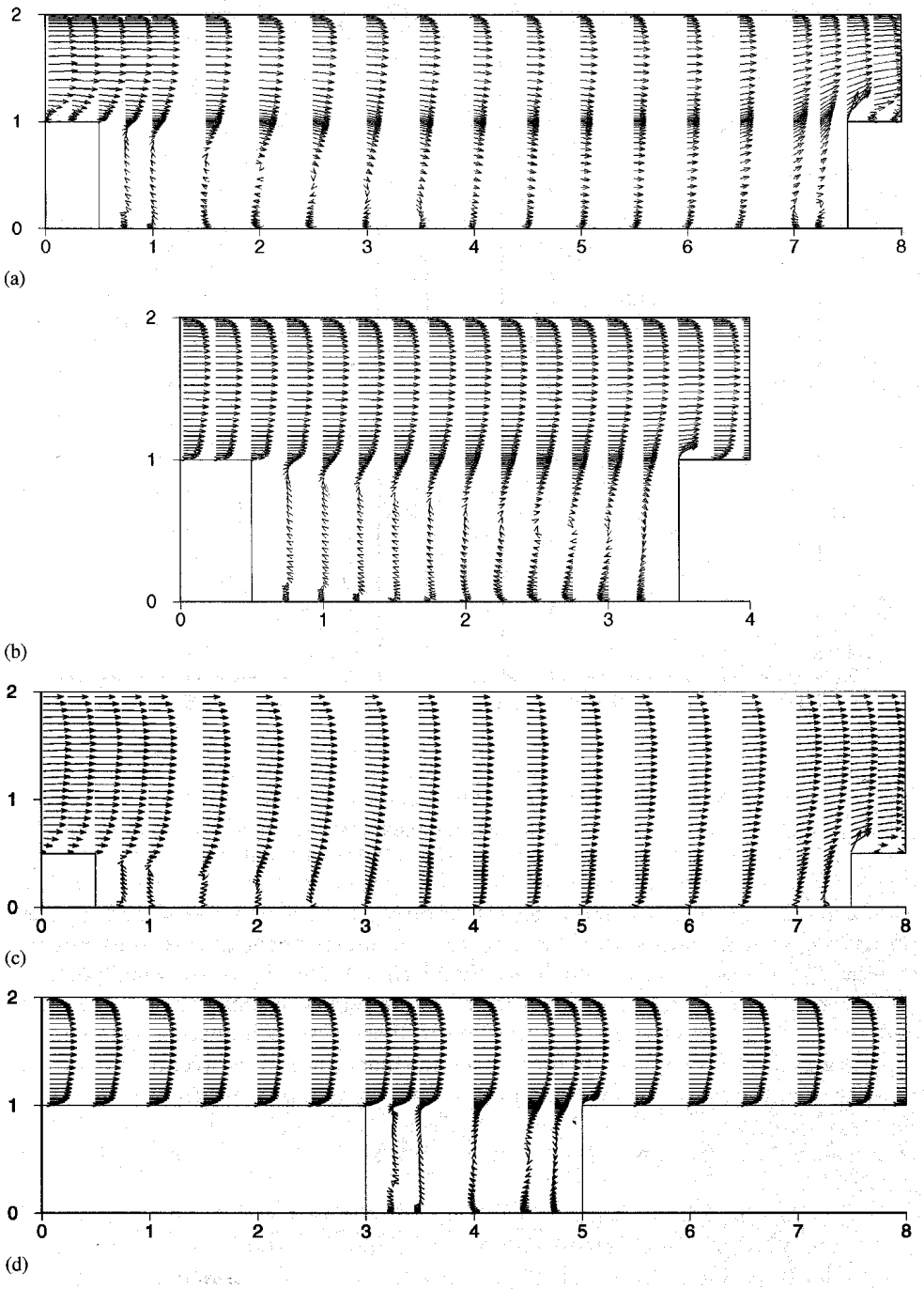

Fig. 7. Velocity vector plots for the averaged flow fields: (a) Case 4; (b) Case 5; (c) Case 6; (d) Case 7.

that the upper downstream corner of the groove of Case 6 is located in the lower part of the streamwise velocity profile than in Case 4.

In Case 7, the main recirculating region is confined in the groove and there is no reattachment present just like in Case 5. The whole flow field is very similar to that of Case 5 in that the flow behaves like the conventional channel flow with the quiet groove region. Therefore, by comparing Case 7 with Case 5, one can notice that the qualitative flow structure does not change as far as L_g is short enough for the main recirculating region to be confined in the groove.

Fig. 8(a), (b), (c) and (d) show the shear-stress (τ_w) distribution both on the top of the protruding surface and on the bottom of the groove for Cases 4, 5, 6 and 7, respectively. The sign of the shear stress accurately determines the location of reattachment. In each case, small secondary structures can be noticed near the lower upstream and the lower downstream corners of the groove. In Cases 5 and 7, the magnitude of τ_w is very small from the upstream vertical wall to the central part of the groove. Furthermore, τ_w is almost constant on the top of the protruding surface, which is consistent with the previous observation that the flow resembles the channel flow between two flat plates $H - h$ apart.

The distribution of total turbulent fluctuation ($\overline{u'^2} + \overline{v'^2} + \overline{w'^2}$) in Cases 3, 4, 5 and 7 is shown in Fig. 9(a), (b), (c) and (d), respectively. The increment in contours is 0.03 in Cases 3, 4 and 7, and 0.06 in Case 5. Solid lines represent higher values than dashed lines. The regions marked by solid lines thus have strong turbulent fluctuations. In all four cases, one can observe strong fluctuations near the upper downstream corner of the groove and in the free-shear layer at the upper boundary part of the groove. In particular, the latter plays an important role in mass and heat transfer to and from the groove. Since there is no flow separation present on the top of the protruding surface in Cases 5 and 7, the free-shear layers in those cases are due to the recirculating flows in the groove. Thus, the region of strong turbulent fluctuation appears slightly towards the downstream part of the groove accordingly. On the contrary, the free-shear layers in Cases 3 and 4 are mainly created by the flow separation near the upper downstream corner of the groove; the region of strong fluctuation is located in the upstream part of the groove in those cases. The turbulent fluctuations are very weak in the groove when the main recirculation is confined (Cases 5 and 7). From this, combined with the previous observation of weak mean flow in the groove, one cannot expect effective mass and heat transfers when the main recirculation is confined.

The seventh column of Table 1 ($\Delta p/\Delta p_{\text{Case 3}}$) represents the dimensionless mean pressure difference between inlet and outlet. Here, $\Delta p_{\text{Case 3}}$ denotes the pressure difference in Case 3, and Δp is the "effective" mean pressure difference for each case, corresponding to the streamwise length of the computational domain of Case 3. As L_g becomes shorter, Δp is increased (Case 4), and then decreased (Case 5) to maintain an approximately constant ("target") level of volume flux (or Re). The decrease of Δp in Case 5 is related to the change of the large-scale flow structure in the groove. Unlike in Cases 3 and 4, the main flow in Case 5 behaves "as if" there were no groove in the flow field. Therefore, a smaller Δp is allowed to maintain the target volume flux in Case 5. This argument can be supported by comparison of Cases 4 and 6. Case 6 is closer to the conventional channel flow than Case 4, and its mean pressure difference

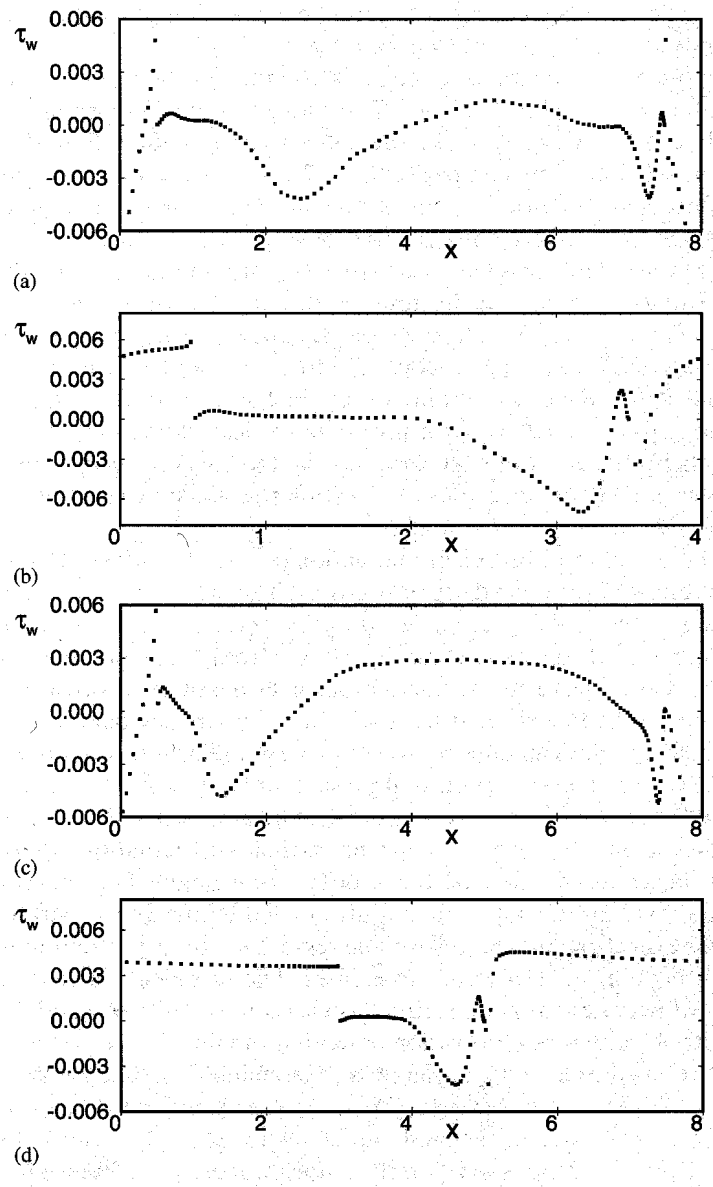

Fig. 8. Distributions of shear stress both on the top of the protruding surface and on the bottom of the groove: (a) Case 4; (b) Case 5; (c) Case 6; (d) Case 7.

is thus much smaller than that of Case 4 (Table 1). In comparison of Case 5 with Case 6, one can also notice that Case 5 requires a bigger Δp than Case 6 to maintain the target volume flux because Case 5 corresponds to a conventional channel flow with a smaller cross-sectional area. A similar argument can be applied to Cases 5 and

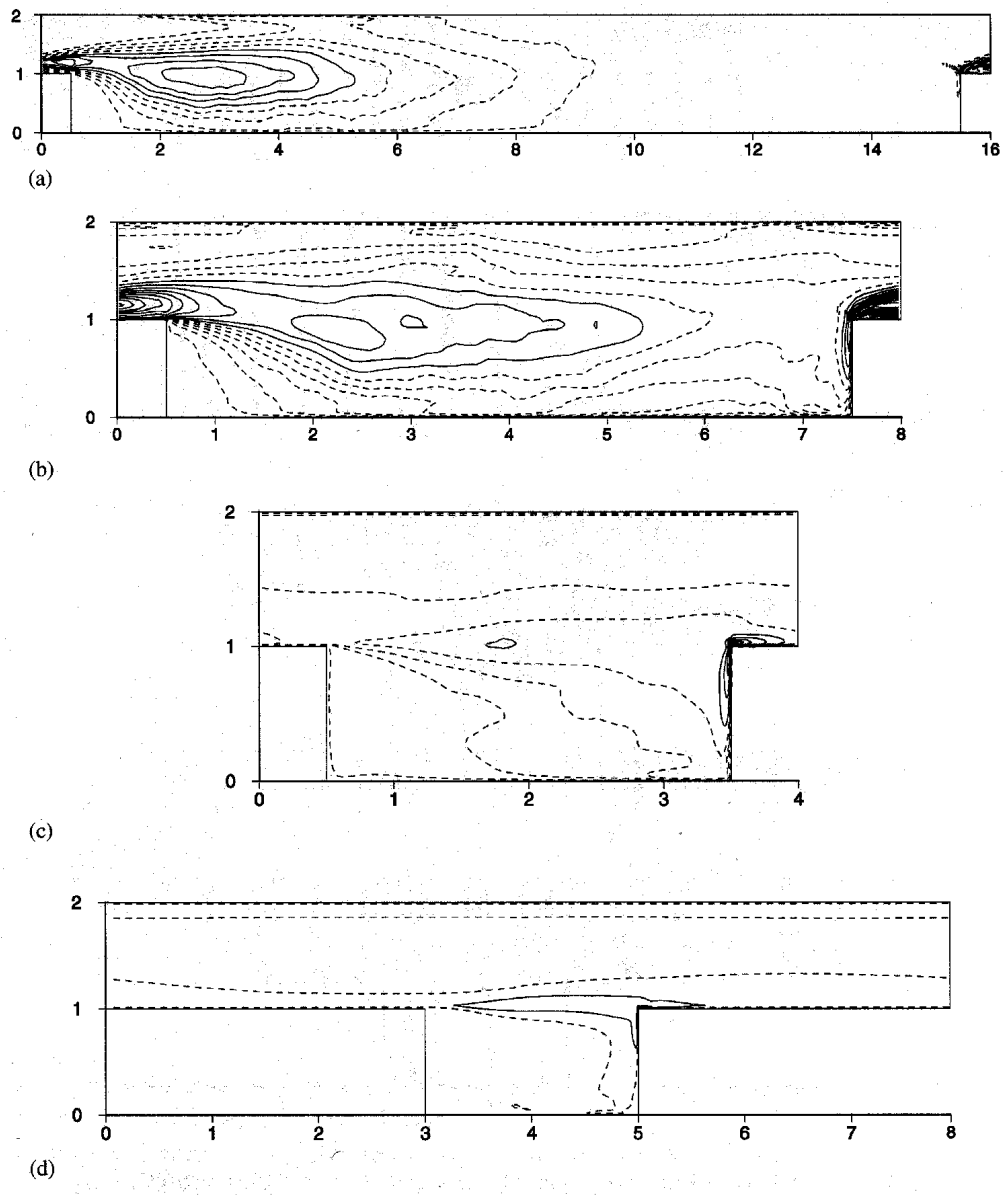

Fig. 9. Contours of total turbulent fluctuation: (a) Case 3; (b) Case 4; (c) Case 5; (d) Case 7.

7, and to Cases 6 and 7. Case 7 is closer to a "channel" flow than Case 5, and Case 6 is corresponding to a channel flow with a wider gap than Case 7. Therefore, Δp of Case 7 is smaller than that of Case 5, and Δp of Case 6 is smaller than that of Case 7. All these trends are consistent with the previous observation of the change of the large-scale flow structures in the groove depending on L_g.

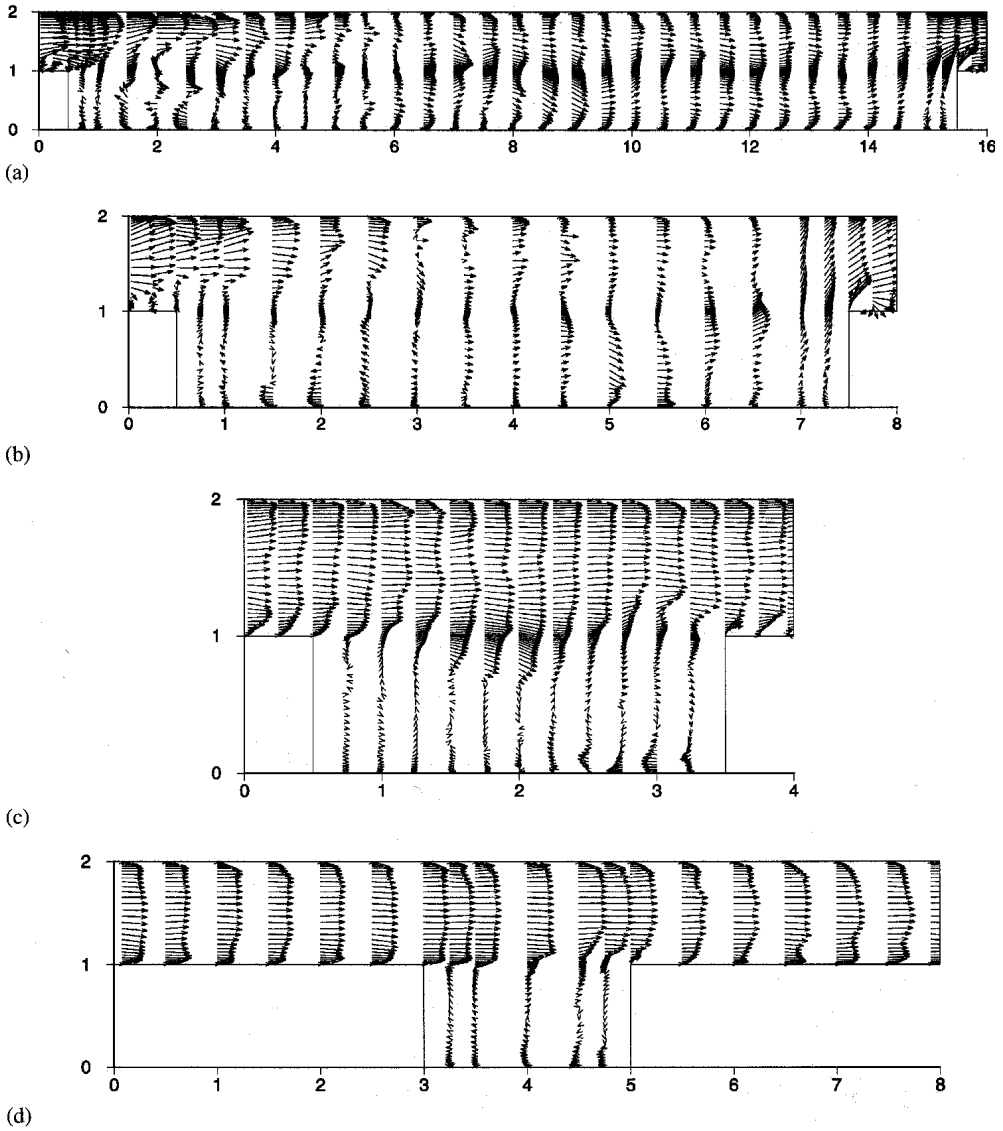

Fig. 10. Instantaneous velocity vector plots: (a) Case 3; (b) Case 4; (c) Case 5; (d) Case 7.

3.2.2. *Instantaneous flow fields*

Fig. 10(a), (b), (c) and (d) show instantaneous velocity vectors on a typical x–y plane for Cases 3, 4, 5 and 7, respectively. The vectors are scaled differently in each figure. In Case 3, one can identify the typical flow structures such as free-shear layers, vortex shedding, recirculation, and reattachment, which are present in the backward-facing step flow. In Cases 5 and 7, however, the vector plots are very much similar to those of averaged fields (Fig. 7(b) and (d)). In particular, the instantaneous recirculating flow in

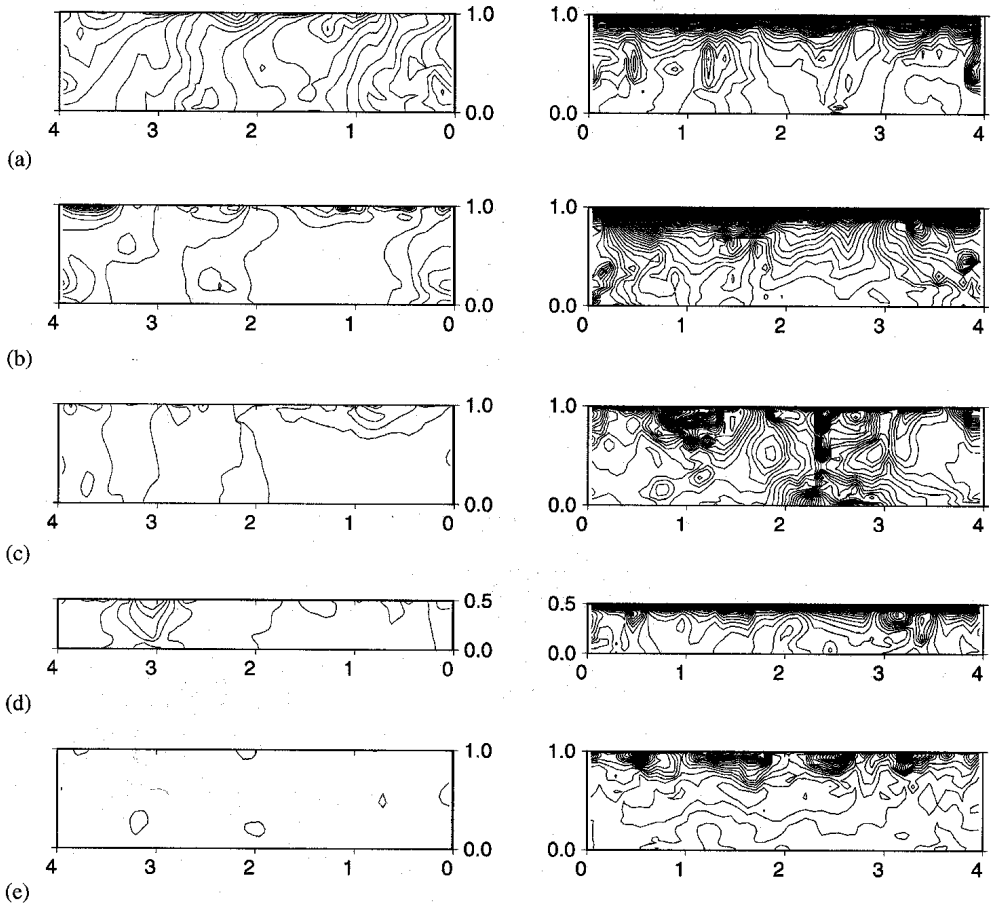

Fig. 11. Contours of pressure on the upstream and the downstream boundaries of the groove: (a) Case 3; (b) Case 4; (c) Case 5; (d) Case 6; (e) Case 7.

the groove is also very weak, and this supports our previous statement that turbulent fluctuations are weak in the groove.

Pressure contours on the upstream and the downstream boundaries of the groove in Cases 3, 4, 5, 6 and 7 are revealed in Fig. 11(a), (b), (c), (d) and (e), respectively, with an increment of 0.02. The horizontal axis represents the z direction. Since the upstream boundary is inside the recirculating region, the pressure gradient on the boundary is small. On the contrary, that is not the case on the downstream counterpart. Especially, in Case 4 where Δp is the biggest of all the cases, the pressure gradient on the downstream boundary is also the highest. In Cases 5 and 7 where L_g is short, the pressure gradient is low on the downstream boundary except near the corner, and is also very low in the upstream counterpart compared with the other cases. This is another evidence that the flow inside the groove is very weak in Cases 5 and 7. The distribution of contours in Case 6 is similar to that of Case 4 with the length scale

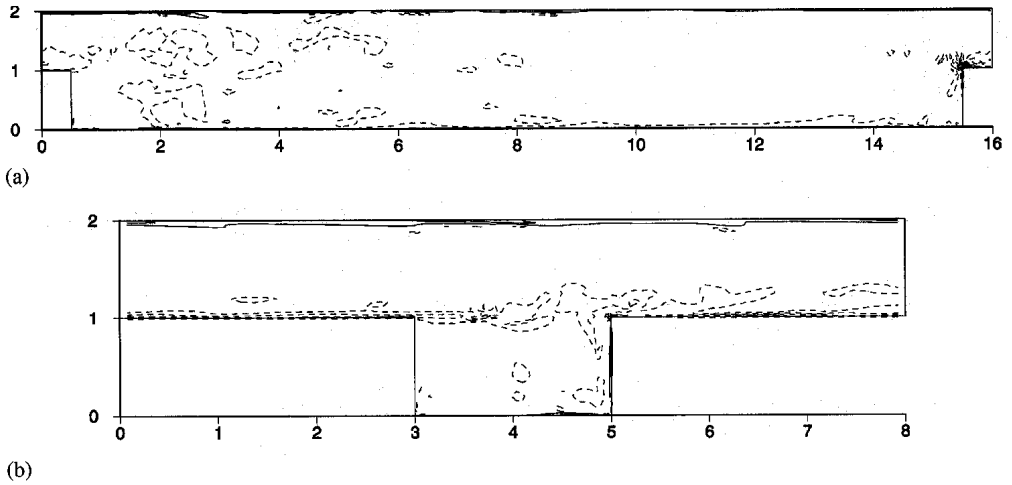

Fig. 12. Contours of instantaneous spanwise vorticity: (a) Case 3; (b) Case 7.

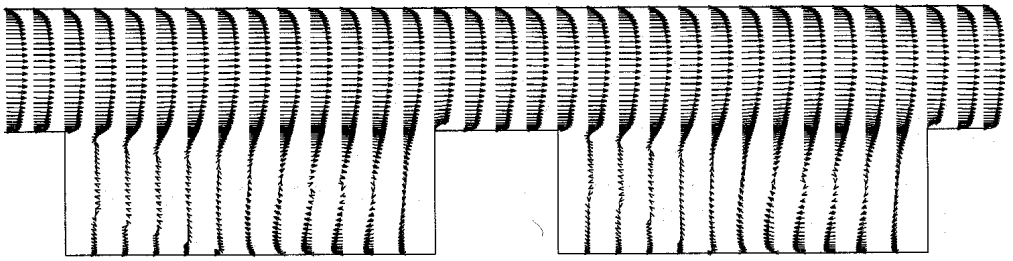

Fig. 13. LES in a domain with two gooves, an averaged field. Re = 10,400.

reduced approximately by half in y. This is consistent with the previous statement that the averaged flow field is scaled to each other in Cases 4 and 6.

Fig. 12(a) and (b) represent the distribution of the spanwise vorticity (ω_z) on a typical x–y plane for Cases 3 and 7, respectively. Solid lines denote positive values, and dashed lines negative values with an increment of 12. In Case 3, the maximum value of ω_z appears near the upper downstream corner of the groove, and ω_z diminishes in the downstream part of the groove. In Case 7, however, ω_z persists in the groove, and its distribution in the groove is consistent with that of the turbulent fluctuation.

3.2.3. *Flow structures of fundamental type*

All the cases mentioned so far were computed with a computational domain containing only one groove. Therefore, flow structures of subharmonic type, if they exist, cannot be detected with such a limited domain. To explore the possibility of existence of subharmonic structures, an additional LES was performed using a computational domain with two grooves. Here, the domain of Case 5 was repeated in the streamwise direction. Case 5 was selected for this test because it has the highest chance of subharmonic structures. Fig. 13 shows the flow field averaged for one FTT with

Re = 10,400. The flow structure in each groove is almost identical. This verifies that there are no subharmonic structures present for the geometries and the Reynolds numbers considered in this study, and supports our approach which focused on the harmonic structures.

4. Conclusion

In this study, turbulent flows in periodically grooved channel were investigated using LES. Especially, a parametric study was performed to investigate the effects of length and depth of a groove on large-scale flow structures. A relatively low Reynolds number was chosen in order to resolve the wall-shear layers with the no-slip boundary condition.

First of all, a DNS was performed to build an accurate set of benchmark data for one test case. Then, performance of LES was evaluated against the DNS data for mean velocities and turbulent fluctuations. A good agreement was obtained even though the number of grid points of LES was only 6.5% of that of DNS. This confirms that LES is a suitable tool for a parametric study of turbulent flows.

Secondly, a parametric study was carried out using LES, and observations were made as follows. When the groove is long enough, there exist the flow structures typically observed in backward-facing step flow, such as free-shear layers, recirculating regions, reattachment and redevelopment, and secondary flows. When the groove is short, the recirculating region is confined in the groove; neither reattachment nor redevelopment occurs. In this case, the recirculation in the groove is very weak, and the whole flow field behaves like a conventional "channel" flow. As a result, the mean pressure difference between inlet and outlet is decreased, and the region of high turbulent intensity appears in the middle of the upper boundary of the groove. Since the weak recirculation occupies the entire groove, one cannot expect effective mass and heat transfers there. When the depth of a long groove varies, the qualitative change of the flow structures is insignificant, but their length scales quantitatively depend upon the groove depth. All these observations were consistently confirmed by both averaged and instantaneous flow fields.

Acknowledgements

This research was financially supported by Korea Science and Engineering Foundation (95-0200-16-01-3). Computations in the present work were carried out by using the CRAY C90' of the ETRI supercomputer center in Korea, which is gratefully acknowledged. A part of computing time used in this study was provided by 1998 Inha University Research Fund.

References

[1] B.F. Armaly, F. Durst, J.C.F. Pereira, B. Schonung, Experimental and theoretical investigation of backward-facing step flow, J. Fluid Mech. 127 (1983) 473–496.

[2] G. Dimaczek, R. Kessler, R. Martinuzzi, C. Tropea, The flow over two-dimensional, surface-mounted obstacles at high Reynolds numbers, The Seventh Symposium on Turbulent Shear Flows, Stanford University, 1989, pp. 10.1.1–10.1.6.
[3] S. Okamoto, K. Nakaso, Turbulent shear flow over rows of two-dimensional square ribs on ground plane, The Eighth Symposium on Turbulent Shear Flows, Technical University of Munich, 1991, pp. 14.3.1–14.3.6.
[4] S. Yamashita, I. Nakamura, T. Kushida, H. Yamada, An experimental study on the separation of a turbulent boundary layer from a sharp edge, The Eighth Symposium on Turbulent Shear Flows, Technical University of Munich, 1991, pp. 17.4.1–17.4.6.
[5] C.H. Amon, Spectral element-Fourier method for transitional flows in complex geometries, AIAA J. 31 (1) (1993) 42–48.
[6] N.K. Ghaddar, M. Magen, B.B. Mikic, A.T. Patera, Numerical investigation of incompressible flow in grooved-channels; Part 2: resonance and oscillatory heat transfer enhancement, J. Fluid Mech. 168 (1986) 541–567.
[7] R.A. Sahan, A. Liakopoulos, H. Gunes, Reduced dynamical models of nonisothermal transitional grooved-channel flow, Phys. Fluids 9 (3) (1997) 551–565.
[8] S. Murakami, Current status and future trends in computational wind engineering, J. Wind Eng. Ind. Aerodyn. (67 and 68) (1997) 3–34.
[9] S. Murakami, Comparison of various turbulence models applied to a bluff body, J. Wind Eng. Ind. Aerodyn. (46 and 47) (1993) 21-36.
[10] K.-S. Yang, J.H. Ferziger, Large-eddy simulation of turbulent obstacle flow using a dynamic subgrid-scale model, AIAA J. 31 (8) (1993) 1406–1413.
[11] J. Kim, P. Moin, Application of a fractional step method to incompressible Navier–Stokes equations, J. Comput. Phys. 59 (1985) 308–323.
[12] M. Germano, U. Piomelli, P. Moin, W. Cabot, A dynamic subgrid-scale eddy viscosity model, Phys. Fluids A 3 (7) (1991) 1760–1765.
[13] D.K. Lilly, A proposed modification of the Germano subgrid-scale closure method, Phys. Fluids A 4 (3) (1992) 633–635.
[14] J. Jimenez, P. Moin, The minimal flow unit in near-wall turbulence, J. Fluid Mech. 225 (1990) 213.
[15] R. Kessler, K.-S. Yang, Direct numerical simulation of turbulent obstacle flow, KSME Int.J. 12 (2) (1998) 291–300.